MURDOCH RESEARCH REPOSITORY

http://ieeexplore.ieee.org/xpl/articleDetails.jsp?arnumber=974051&contentType=Conference+Publications

Kwok, S.M., Chandrasekhar, R. and Attikiouzel, Y. (2001) Automatic pectoral muscle segmentation on mammograms by straight line estimation and cliff detection. In: The Seventh Australian and New Zealand Intelligent Information Systems Conference, 18 - 21 November, Perth, W.A, pp. 67-72.

http://researchrepository.murdoch.edu.au/19618/

Copyright © 2001 IEEE

Personal use of this material is permitted. However, permission to reprint/republish this material for advertising or promotional purposes or for creating new collective works for resale or redistribution to servers or lists, or to reuse any copyrighted component of this work in other works must be obtained from the IEEE.

Automatic Pectoral Muscle Segmentation on Mammograms by Straight Line Estimation and Cliff Detection

S M Kwok, R Chandrasekhar and Y Attikiouzel
Australian Research Centre for Medical Engineering (ARCME)
The University of Western Australia
35 Stirling Highway, Crawley, WA 6009
Australia
kwok-sm@ee.uwa.edu.au | chandra@arcme.uwa.edu.au | yianni@arcme.uwa.edu.au

Abstract: Mammograms, which are X-ray images of the female breast, are used widely by radiologists to screen for breast cancer. The first stage of any computerized analysis of the digitised mammogram is to divide the image into anatomically distinct regions. The pectoral muscle is one of these regions and it appears on mediolateral oblique views of mammograms. In this paper, the rationale and algorithms for fully automatic, two-part segmentation of the pectoral muscle are presented. The algorithm consists of (a) estimation of the muscle edge by a straight line; and (b) refinement of the detected edge by surface smoothing and edge detection in a restricted neighbourhood derived from the first estimate.

1 Introduction

Film-screen X-ray mammography is a standard breast imaging technique used worldwide to detect breast cancer. Computers may be used to analyse digitised mammograms for the purpose of assisting radiologists. The first stage in mammogram analysis usually involves segmenting the image into several distinct regions, including the breast border [1], the nipple [2] and the pectoral muscle, which only appears on mediolateral oblique views of mammograms. The edge of the pectoral muscle is useful in determining mammogram adequacy [3], mammogram-pair registration and comparison [4], and for restricting the search space for lesion detection [5]. In this paper, we describe a fully automatic method for pectoral muscle segmentation, based on intensity thresholding, straight line fitting, surface smoothing and edge detection.

2 Overview of Algorithm

The algorithm consists of two parts: straight line *estimation* and *cliff detection*. Although the pectoral muscle edge, or *pectoral margin* is not necessarily a straight line, it may usefully be modelled as one in a first estimate. The second part embodies refinements to more accurately reflect the possible non-linear contour of the pectoral edge. The search for the true edge is now localized to a neighbourhood defined by the initial straight line estimate, and model-based edge detection and interpolation are used to determine the final edge.

3 Straight Line Estimation

The pectoral margin is estimated initially as a straight line. The Hough transform [6, 7] has been cited as a simple way to detect straight line features on mammograms. Here we describe a method based on iterative thresholding and a gradient test. The result is verified by an independent method.

3.1 Orientation and Notation

The original image is first oriented so that the pectoral muscle is located at the top left corner (i.e., all right breast images are mirrored vertically). Images have a bit-depth of 8-bits grey scale [0-255] and resolution is 400 micrometres per pixel. The intensity or pixel value of the image is denoted as $I(x, y)$ with the origin at the top-left corner of the image (see Figure 1). The x-axis represents the top edge pointing to the right, while the y-axis represents the left edge running downwards. The number of pixels of the image in the x- and y-directions are denoted by n_x and n_y, respectively. For algorithms in the Euclidean 2D space, y is used as the independent variable rather than x.

3.2 Assumptions

Three assumptions were made about the pectoral muscle:

1) The muscle is located (partially, if not fully) in the *top left quarter* of the image, touching the top and left edges.
2) The straight line estimating the muscle edge

intersects the top and left edges of the image inside the breast region.

3) The intensity of the muscle is generally higher than that of the adjoining parenchyma.

3.3 Region of Interest (ROI)

The Region of Interest (ROI) is a subset of the image with rectangular shape. It defines the region where we expect to find the muscle edge; hence anything outside of the ROI is ignored. In accordance with assumption 1, the first ROI, R_1, is initially set to the *top left quarter* of the image:

$$R_1 = \{(x,y): 0 \le x < n_x/2 \text{ and } 0 \le y < n_y/2\} \quad (1)$$

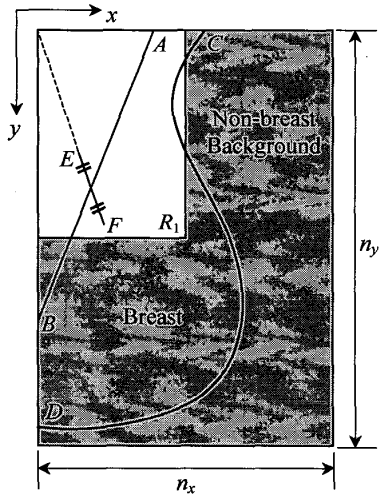

Figure 1: The breast is orientated so that the pectoral muscle is located at the top-left corner. The coordinates axes are directed as shown with the origin also at the top-left corner. The width of the whole image is n_x and the height is n_y. R_1 is the initial region of interest (ROI). The straight line $\overline{AB}$ approximates the muscle edge. Points C and D are the end-points of the breast border. Line $\overline{EF}$ is a search path.

3.4 Iterative Thresholding

Figure 2a shows the initial ROI, R_1, of mammogram mdb227 taken from the MIAS database [8]. Iterative thresholding [9] is performed in this ROI as follows:

1) R_1 may contain some portion of the non-breast background, which lies to the right of the curve CD in Figure 1. These intensities should be excluded from iterative thresholding. They are assumed to lie *below* some threshold t_e.
2) Set the threshold t to be the mean of all remaining pixel values in R_1:

$$t = \sum_{i \ge t_e} z_i n(z_i) \Big/ \sum_{i \ge t_e} n(z_i) \quad (2)$$

where $n(z_i)$ is the number of pixels with intensity z_i in R_1.

3) Threshold the ROI at t to label the object and the background.
4) Compute the means of the pixel values of the object and the background, denoted by μ_o and μ_b respectively. Then update t by:

$$t = \frac{\mu_o + \mu_b}{2} \quad (3)$$

5) If the new t remains unchanged, it is the final threshold; otherwise repeat steps 3 to 5.

A binary image is obtained by labelling all pixel values larger than t as the *pectoral region*, and everything else as the *parenchymal region* (see Figure 3a). Finally we remove noise on this binary image by applying a 5 × 5 median filter.

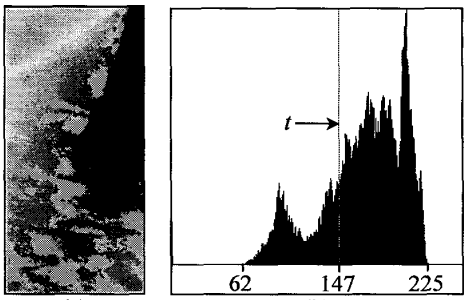

Figure 2: (a) ROI of MIAS image mdb227. (b) Histogram of the ROI where the vertical grey line indicates the optimal threshold t for this image.

3.5 Line Fitting with Gradient Test

There are five steps to fit a straight line to the border between the pectoral and parenchymal regions.

3.5.1 Pixel Selection

1) Scan horizontally from left to right on the image. In each scan line, select the *first* pixel belonging to the parenchymal region. All the selected points form the function $M_1(y)$ representing the muscle edge.

Note that for clear pectoral margins the iterative thresholding separates the pectoral muscle well and hence $M_1(y)$ represents the pectoral margin well. However the curve $M_1(y)$ deviates towards the parenchyma and forms a concave segment whenever the glandular tissues overlap the mus-

cle edge (see Figure 3a). For this reason, we carry out a *gradient test* on $M_1(y)$ to eliminate problematic portions of $M_1(y)$.

3.5.2 Gradient Test

2) Gradient test:
   a) Slide a window of height $w = n_y/10$ and width equal to the ROI, downward along the y-axis (see Figure 3b).
   b) Fit a straight line to $M_1(y)$ inside this window.
   c) Compute the gradient, $g(y)$, of the line.

$$g(y) = \frac{\Delta x}{w} \quad \text{for } \frac{w}{2} < y < n_y - \frac{w}{2} \qquad (4)$$

Thus the gradient is known for each segment of $M_1(y)$. Negative gradient represents the correct form of muscle edge while positive gradient indicates that non-pectoral tissues have been included in the pectoral region.

3.5.3 Straight Line Fitting

3) Set all the segments with positive gradient to zero to form $M_2(y)$.
4) In $M_2(y)$, there are a number of segments left. Choose the one with the largest area under the curve (shown shaded in Figure 3c) to form $M_3(y)$.
5) Fit a straight line to minimise the least squared error to $M_3(y)$. This line, denoted by $M_E(y)$, is shown as $\overline{AB}$ in Figure 1. It is the *first* approximation to the muscle edge.

Figure 3 illustrates steps 1 to 5.

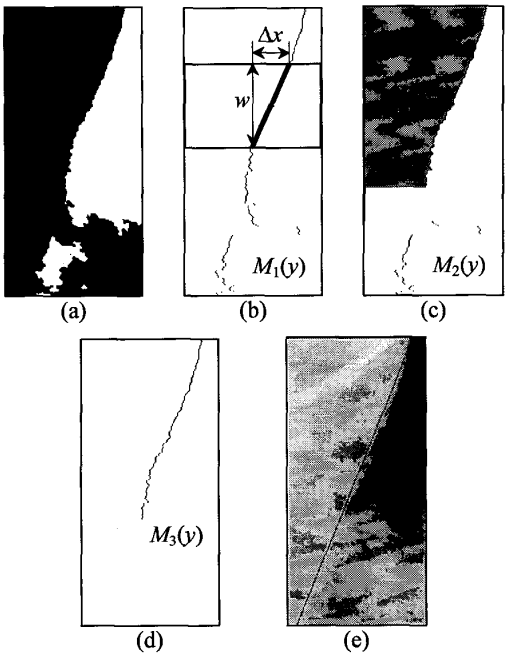

Figure 3: (a) Median filtered binary image of ROI of mdb227 where the pectoral region is black and the parenchymal region is white. (b) $M_1(y)$ obtained by tracing the edge of black region. (c) $M_2(y)$ obtained by removing segments with positive gradient. (d) $M_3(y)$ obtained by selecting the largest area under the curve, which is the shaded region in (c). (e) Line fitted to $M_3(y)$ shown superimposed on original image. Note that the glandular tissues overlap the pectoral muscle causing bad thresholding in the binary image (a).

3.6 Validation

A bad straight line estimate can lead to an even worse result in the detection step. Thus the line $\overline{AB}$ (or equivalently, $M_E(y)$) is *independently* validated at least twice before the second stage of the algorithm. Validation is based on assumption 2. Line $\overline{AB}$ is valid if it intersects the top and left edges of the image inside the breast region, and not valid otherwise,

$$\text{i.e.,} \quad 0 < x_A < x_C \quad \text{and} \quad 0 < y_B < y_D \qquad (5)$$

where $(x_A, 0)$ is point A, $(0, y_B)$ is point B, $(x_C, 0)$ is point C and $(0, y_D)$ is point D in Figure 1. Because the breast border was extracted automatically by polynomial modelling (described in [1]), tapes or labels could affect it. So points C and D have to be obtained as:

$$x_C = \max\{x_{\text{border}} : 0 \le y_{\text{border}} \le 0.15 n_y\} \qquad (6)$$
$$y_D = \max\{y_{\text{border}} : 0 \le x_{\text{border}} \le 0.15 n_x\} \qquad (7)$$

The straight line estimate is validated several times in the following procedure:

1) Validate $M_E(y)$. If it is valid go to step 2, otherwise go to step 3.
2) A second estimation is performed in a new ROI, $\hat{R}_1$, which is resized so that $\overline{AB}$ runs diagonally from the top right corner to the left bottom corner:

$$\hat{R}_1 = \{(x, y): 0 \le x < x_A \text{ and } 0 \le y < y_B\} \qquad (8)$$

   Repeat the steps outlined in sections 2.4 to 2.5 for the new ROI, $\hat{R}_1$, to get a *second* estimate for $M_E(y)$, or $\overline{AB}$. If the second line is also valid, it is taken to be the final straight line estimate and the algorithm stops; otherwise it continues to step 3.
3) Make the ROI smaller by taking the top left quarter of R_1 and go back to step 1. However, if the new ROI is smaller than 1/256 of the original image, exit the algorithm.

This validation is very important to our algorithm. It ensures that the *direction* of the straight

line $M_E(y)$, is correct and by inference, that both the threshold t and the fitted straight line are good estimates. When $M_E(y)$ is verified to be not valid, 3 cases are most likely:

1) The pectoral muscle *does not exist* in the mammogram.
2) The pectoral muscle is so *small* that the wrong threshold value was determined.
3) The pectoral muscle is *very large and curved*, so that although the correct straight line is estimated, it intersects the top or left edge *outside* the breast region.

When validation fails, it is assumed that case 2 above applies, and the ROI is reduced accordingly. Repeated estimation and validation are attempted with progressively smaller ROIs, up to 3 times, until the ROI is shrunk down to 1/256 of the original image. If a valid straight line estimate cannot still be found, either case 1 or 3 is assumed. The algorithm then exits with a warning message concerning that the pectoral margin is absent. This may signify an *inadequate* mammogram, as noted in reference [10], which states "the pectoralis muscle should be visualized to approximately the level of the nipple".

4 Cliff Detection

Cliff detection is designed to *refine* the muscle edge along the straight line estimate $\overline{AB}$, because the actual muscle edge may be slightly curved. Two major components in cliff detection are *surface smoothing* and *edge detection*. Surface smoothing is used *to remove noise and rough texture* on the intensity surface model whereas edge detection is used to find the *real shape* of the muscle edge within a *detection range*.

4.1 Surface Smoothing

There are several methods to smooth the intensity surface including mean filtering, Gaussian filtering, polynomial fitting and bicubic spline interpolation. Each of these methods was individually tested; it was found that mean filtering followed by bicubic spline interpolation was most useful for our purpose. The procedure is as follows:

1) To reduce computational time, set the ROI to:

$$R_d = \{(x, y): 0 \le x \le x_A + d \text{ and } 0 \le y \le y_B + d\} \quad (9)$$

where d defines the *detection range* explained in Section 4.2.

2) Smooth R_d by a mean filter, in the spatial domain, of size $m \times m$.
3) Sub-sample pixels in R_d using a sampling interval of s pixels, i.e., take every s-th pixel along the x and y directions, and form a rectangular grid. If x_A or y_B is smaller than s, sub-sampling is not possible, so skip steps 3 and 4.
4) Apply bicubic spline interpolation to the sampling points to reconstruct a surface model of high order of smoothness. Details of implementation are described in reference [11, pp. 109-110].

4.2 Edge Detection

Edge detection is used to locate the *exact position* of the muscle edge using (a) the *straight line estimate*, $M_E(y)$, of the pectoral margin as a guide and (b) the *smoothed intensity surface* to which bicubic spline interpolation has been applied, as described in section 4.1.

1) Define a *detection range* (see Figure 1 and 4a): From each point on the line $\overline{AB}$ (or equivalently, $M_E(y)$), construct an imaginary line through the origin and set the *search path* to length $2d$ so that the distances on both sides of $\overline{AB}$ are equal. For example, $\overline{EF}$ in Figure 1 is a search path. It is better to define the search paths in this way rather than perpendicularly because the search path lengths are then not reduced at the image edges.
2) Search for the intensity cliff caused by the intensity drop along the muscle edge. For each search path within the detection range, extract the intensity profile denoted by $I_p(k)$.
3) Fit a sigmoid to $I_m(k)$ to $I_p(k)$ so that the absolute error, $|\varepsilon| = |I_m(k) - I_p(k)|$, is minimised. The sigmoid may be a hyperbolic tangent:

$$I_m(k) = \frac{I_{p,\max} - I_{p,\min}}{2} \tanh\left((\alpha - k)\frac{4}{d}\right) + \frac{I_{p,\max} + I_{p,\min}}{2}$$

for $0 \le k \le 2d$ and $\alpha \in [0, 2d]$ (10)

where $I_{p,\max}$ and $I_{p,\min}$ are the maximum and minimum intensities in $I_p(k)$.

4) The cliff is located at the *point of inflection of the model* because the gradient magnitude (or intensity drop) at this point is largest.

There are two advantages to cliff detection:

1) Cliff detection ignores intensity rise and only detects intensity drop.
2) By virtue of the fitted model, cliff detection is more robust to noise and bright spots on the image; hence it gives fewer scattered and broken edges.

4.3 Region Enclosing

The edges given by cliff detection may be discontinuous (see Figure 4b) so that the final pectoral

margin does not form a closed triangle. These are therefore linearly interpolated [11, pp. 94], with y as the independent variable, to form an enclosed region. If there is more than one data-point lying on any horizontal scan-line, the point with the greatest x value is taken. The curve resulting from linear interpolation is further smoothed by a moving-window mean filter, of length ℓ pixels. Figure 4c shows an example of the enclosed region resulting from the final segmentation.

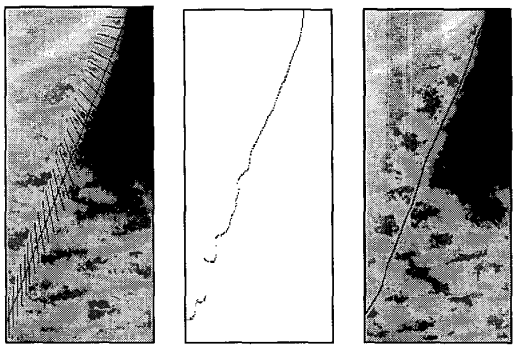

(a) (b) (c)

Figure 4: (a) Detection range with search paths pointing to top-left corner (only every tenth path is shown). (b) Resulting edges from cliff detection. (c)The closed triangular region is the final segmentation of the pectoral muscle.

5 Experimental Method

This algorithm has been tested on all 322 images from the MIAS database. The original 50 μm/pixel images were low-pass filtered and reduced in resolution to 400 μm/pixel. The threshold t_e was set conservatively to 38, which is 15% of the maximum possible intensity (equal to 255 in our case). The parameters used in the algorithm were expressed in terms of n_y to achieve generality:

$$w = 0.1n_y \quad ; \quad m = 0.02n_y \quad ; \quad s = 0.02n_y$$
$$d = 0.04n_y \quad ; \quad \ell = 0.12n_y$$

Therefore the algorithm is adaptive to different image resolutions.

6 Results

As a preliminary evaluation, the first author gauged the results. Each image was given *two scores* (0 to 5 corresponding respectively to no segmentation, terrible, poor, satisfactory, good, excellent) — one for the straight line estimation and one for the cliff detection.

1) The average score for straight line estimation is 4.35 and for cliff detection is 4.41. They indicate that the results are generally good and that the method works.
2) The correlation coefficient between estimation and detection is 0.95, indicating a strong directly proportional relationship between these two processes. Results show that a good detection can correct the small errors made by estimation, thereby achieving refinement. However, a strong detection cannot recover from a very poor estimation, where the pectoral margin lies outside the detection range. In such cases, large errors can propagate through, giving very poor results.
3) Valid straight line estimation could not be achieved for 5 images (mdb153, 179, 236, 287 and 288); they were all scored zero. Among them, mdb236 was the only mediolateral oblique image where the pectoral muscle was absent.

7 Discussion

Figure 5 shows some of the good (a-c) and bad (d-f) results of final segmentation of the pectoral muscle. In those images where the pectoral muscle is clear and separated from glandular tissues, the resulting curves are very accurate, e.g. (a) and (b). The algorithm is not affected by tapes, as shown in (a), (c) and (d), because the search paths at the top are horizontal. It is also robust to artifacts as shown in (b). In (c), the lower half of the pectoral edge is obscured by other tissues, causing uncertainty in the edge detection. Although the exact muscle edge could not be detected, the straight line estimate was followed, and the final result was acceptable. Note that in this image, there is a strong *internal edge* inside the pectoral region. It is the same for (d), but the line was fitted to the internal muscle edge in the latter case. The line fitting decision depends on the binary image produced by iterative thresholding. The pectoral muscle in (e) is quite curved, vertically directed in parts, and mostly indistinct, resulting in a poor segmentation. The results are even worse for (f), which is a particularly difficult image.

8 Conclusions

We have described a method for fully automatic segmentation of the pectoral muscle on oblique-view mammograms. The method contains two major parts: (a) straight line estimation and (b) cliff detection. Straight line estimation includes iterative thresholding and straight line fitting with

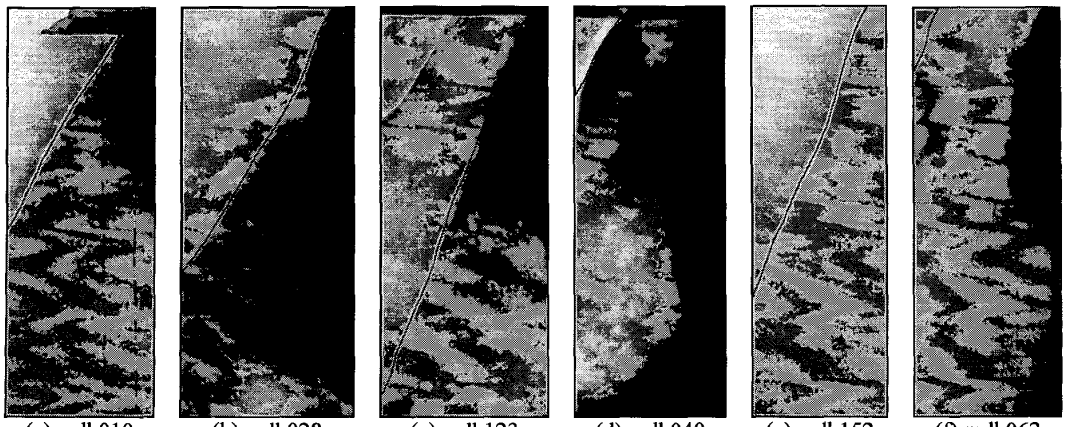

(a) mdb010 (b) mdb028 (c) mdb123 (d) mdb040 (e) mdb152 (f) mdb062

Figure 5: Final segmentation of the pectoral muscle. All images are shown at the same resolution: (a-c) are the good results and (d-f) are the bad ones.

gradient test. This estimate of the pectoral edge is validated at least twice. Cliff detection uses the estimated straight line in conjunction with surface smoothing and edge detection to yield the final segmentation. It was found that bicubic spline interpolation was useful in smoothing the intensity surface while sigmoidal model fitting to intensity profiles across the estimated edge help in locating the pectoral edge more accurately. The method was tested on all images in the MIAS database. Approximately 94% of images were considered acceptably segmented.

9 Acknowledgements

This research was supported in part by Australian Research Council (ARC) Large Grant No. A00000714 and by the Western Australian Government through funding of ARCME as part of its *Centres of Excellence* programme.

10 References

[1] Chandrasekhar R., Attikiouzel Y. "Automatic Breast Border Segmentation by Background Modelling and Subtraction", in *IWDM 2000: 5th International Workshop on Digital Mammography,* (Yaffe M. ed.), Medical Physics Publishing, Madison, USA, 2001, pp. 560-565.

[2] Chandrasekhar R., Attikiouzel Y. "A Simple Method for Automatically Locating the Nipple on Mammograms", *IEEE Transactions on Medical Imaging,* vol. 16, Oct. 1997, pp. 483-494.

[3] Eklund G. W., Cardenosa G., Parsons W. "Assessing Adequacy of Mammographic Image Quality", *Radiology,* vol. 190, Feb. 1994, pp. 297-307.

[4] Tabar L., Dean P. B. *Teaching Atlas of Mammography,* 2nd revised ed. Thieme-Stratton, New York, 1985.

[5] Chandrasekhar R., Attikiouzel Y. "Mammogram-attribute database: A tool for mammogram segmentation and analysis", *Proceedings of the IASTED International Conference: Signal Processing, Pattern Recognition, and Applications,* ACTA Press, Canada, 2001, pp. 143-148.

[6] Chandrasekhar R. *Systematic Segmentation of Mammograms.* PhD Thesis, Centre of Intelligent Information Processing Systems, Dept. of Electrical and Electronic Engineering, The University of Western Australia, Nedlands, Australia, 1996, pp. 143-163.

[7] Karssemeijer N. "Automated classification of parenchymal patterns in mammograms", *Physics in Medicine and Biology,* vol. 43, no. 2, Feb 1998, pp. 365-378.

[8] Suckling J., Parker J., Dance D., Astley S., Hutt I. et al., "The Mammographic Image Analysis Society Digital Mammogram Database", in *Digital Mammography,* pp. 375-378, Elsevier Science, 1994.

[9] Sonka M., Hlavac V., Boyle R. *Image Processing, Analysis, and Machine Vision,* 2nd ed. PWS Publishing, Pacific Grove, 1999.

[10] Peters M. E., Voegeli D. R., Scanlan K. A., eds., *Handbook of Breast Imaging.* Handbooks of Diagnostic Imaging, New York, Churchill Livingstone, 1989.

[11] Press W. H., Flannery B. P., Teukolsky S. A., Vetterling W. T. *Numerical Recipes in C: The Art of Scientific Computing.* Cambridge University Press, Cambridge, 1988.